UHF Propagation Along a Cargo Hold on Board a Merchant Ship

Xiao Hong Mao, *Student Member, IEEE*, and Yee Hui Lee, *Senior Member, IEEE*

***Abstract*—The characterization of a Line of Sight (LOS) and a Non-Line of Sight (NLOS) link is performed over the military Ultra High Frequency (UHF) band (225 to 450 MHz). This is done using experimental results collected inside the cargo hold of a merchant ship. By analyzing the guiding effect associated with the cargo hold and its sub-structures, the channel characteristics of the environment can be determined. This important propagation mechanism is analyzed using the 3-D ray tracing simulator. Path loss for both topologies is studied and linear path loss models are proposed. Small-scale channel characteristics, such as the number of multipath components, decay factor of the multipath components and Root-Mean-Square (RMS) delay spread are studied and compared for the LOS and NLOS scenarios. Due to the guiding effect and multiple reflections along the cargo hold, both the LOS and NLOS scenarios are found to exhibit similar channel characteristics. A linear decay function is proposed to model the average Power Delay Profiles (PDPs). It is concluded that the linear model provides a good representation for the shape of the impulse responses for a cluttered environment with reflective substructures. This study is useful for the implementation of wireless sensor networks for status monitoring in maritime applications.**

***Index Terms*—3-D ray tracing, cargo hold, metallic structure, waveguide effect, wireless sensor network.**

I. Introduction

Wireless propagation in shipboard environments is important for both military and commercial applications. For military applications, in order to seize control of a ship, it is critical to establish a wireless communication link between the bridge and the engine control room. For commercial applications, wireless communication in and out of the cargo hold and within the cargo hold is important. For example, during the loading and unloading of hazardous goods, communication between crew members in and out of the cargo hold is essential for safety reasons. Within the cargo hold, wireless sensor network can be used to monitor the transportation of perishable and hazardous items [1].

In [2]–[9], channel sounding on board different types of ships have been reported. Of these literatures, four of them are on propagation within naval ships (including warships) [2]–[5]. In [2], narrowband channel measurements were performed in the frequency band of 800 MHz to 2500 MHz in order to investigate the signal level of transmission from one compartment to another within a naval ship. They concluded that the rubber door gaskets and other non-conductive structures may be the source of bulkhead penetration. In [3], narrowband channel sounding was performed in the frequency range of 800 MHz to 3 GHz in order to model the opened/closed door effect and polarization effect on the received power level for different transmitter to receiver locations (with a maximum distance of 5 m) onboard a warship. It was found that a closed water tight door can result in a signal strength drop from 5 to 30 dB. No significant depolarization effect was reported. In [4] and [5], wideband channel characteristics were examined using the Vector Network Analyzer (VNA). In [4], the channel impulse responses on board a warship at 2 GHz and 5 GHz were presented for two scenarios; transmission within compartments; and transmission along a passageway. Based on the received power levels, it was concluded that it is possible to use wireless LAN onboard a warship. However, due to the significant amount of multipath components within the complex environment of the warship, the transmission bandwidth is limited. In [5], wideband measurements were carried out inside compartments and along the starboard corridor of a naval ship within the frequency range of 800 MHz to 2.6 GHz. It was found that the delay spread obtained is large while the path loss exponent is small. These findings are independent on frequency over the band of interest. In these reported work, since the dimensions of the watertight compartments and the corridor within the naval ships and warships are small; the separation between the transmitter and receiver distance is therefore small. However, the dimensions within the cruise ship are generally larger and therefore, their channel characteristics are expected to be different. In [6] and [7], path loss in a restaurant hall and along a cabin corridor on board a cruise ship at 2.4 GHz was studied based on measurement results in the frequency domain. It was found that the path loss in the restaurant hall can be modeled as free space propagation. The path loss along the cabin corridor can better be modeled as dual-slope decay propagation. In [2]–[7], same deck propagation onboard ships were studied. In [8] and [9], inter-deck propagation onboard a merchant ship was investigated. In [8], the propagation mechanisms at 255.6 MHz associated with the channel along the lift shaft that connects the top deck and the bottom deck of the ship were discussed. Due to the guiding effect of the lift shaft and the rich multipath components from the complex metallic ship structure, the delay spread was found to be large. In [9], the feasibility of broadband communication in the military UHF band between two locations with large distance separation within the ship,

Manuscript received April 12, 2011; revised November 1, 2011 and May 10, 2012; accepted September 3, 2012. The associate editor coordinating the review of this paper and approving it for publication was D. Michelson.

This work was supported in full by the Advanced Communications Research Program DSOCL06271, a research grant from the Directorate of Research and Technology (DRTech), Ministry of Defence, Singapore.

The authors are with the School of Electrical and Electronic Engineering, Nanyang Technological University, Singapore, 639798 (e-mail: xhmao@ntu.edu.sg; eyhlee@ntu.edu.sg).

Digital Object Identifier 10.1109/TWC.2012.121112.110675

i.e. the cargo hold and the bridge was examined. The guiding effect along the cargo hold was identified from the periodic nature of the received signals.

There is limited or no literature found on wireless radio propagation within the cargo hold. Due to its unique analogous waveguide structure, the channel characteristics of the cargo hold is different from those reported in the above literature. Channel modelling of similar metallic environment such as factories is well established. Radio channel within factories [10]–[15] are found to behave very differently from channels within office buildings because of the open building layouts, the presence of machineries, and the presence of highly reflective materials within the factories. As the material for both the factory and the cargo hold are metal, rich multipath components are expected for both environments. However, there are more metallic machineries present in factories and therefore, more multipath components are expected. In other words, multipath propagation within factories is mainly due to reflections from metallic machineries (impulsive), whereas propagation within the cargo hold is mainly due to its guiding effect (diffusive). This study helps to provide guidelines for the design of a wireless sensor network within the cargo hold of a merchant ship.

In this paper, wideband channel measurement within a cargo hold onboard a merchant ship in the UHF band is presented. Based on the measurement results, propagation mechanisms are identified; the guiding effect of the cargo hold and its substructures is studied and compared with 3-D ray tracing simulation results. Path loss models (large-scale channel characteristics) are proposed. Small-scale channel characteristics such as the number of multipath components, relationship between the strength of the multipath component and its delay and RMS delay spread are modelled and compared for both LOS and NLOS scenarios. The linear decay function is proposed to model the single cluster PDP in a cluttered environment. The parameters presented serve as guidelines for the implementation of wireless sensor networks in the cargo hold for monitoring purpose. The analysis of propagation modes helps to explain both the large-scale and the small-scale channel characteristics obtained from the channel sounding. The similarities between the channel performance of the cargo hold and the factory environment is also compared.

The paper is organized in the following manner: Section II describes the measurement campaign and simulation setup. Channel characterization for both the LOS and NLOS scenarios are presented in Section III. Propagation modes along the cargo hold are studied and compared with the 3-D ray tracing simulation results. Path loss is studied for both scenarios. Small-scale channel characteristics, such as the number of multipath components, the statistical linear model of power delay profile, as well as the delay spread for the LOS and NLOS scenarios are compared. The conclusion of the findings is presented in Section IV.

II. Channel Measurement and Simulation

A. Measurement Campaign

The measurement campaign is performed inside a cargo hold of a docked merchant ship. Fig. 1(a) shows side and top view of the cargo hold. The central part of the cargo hold is the area used for the storage of cargos. As shown in the figure, there are four sets of doors from the top deck that open into the cargo hold during loading and unloading. The dimensions of the main part of the cargo hold are approximately 130 m by 22 m by 5 m (Length x Width x Height). Other areas of the cargo hold are used to store machineries such as fork lift. The measurement campaign is conducted in the cargo area as shown in Fig.1(b). Fig. 1(b) plots the LOS and NLOS setup in the detailed layout of the cargo area. Within the cargo hold, most if not all surfaces and substructures are metallic. As shown in Fig. 1(b), substructures within the cargo hold are four metallic compartments, six pillars and a metal wall. There is no cargo within the cargo hold during the experiment. Compartments 1, 2 and 4 are small service areas situated within the cargo hold. They contain lighting cables, power sockets and tools. Their dimensions are 24.7 m by 7.8 m by 2 m, 9.1 m by 2 m by 2 m, and 8.1 m by 12 m by 2 m (length x width x height) respectively. Compartment 3 is the storage area for power generators. Its dimensions are 4.7 m by 3 m by 2 m (length x width x height). All pillars and walls are made of metal and extend from the top of the cargo hold to the bottom. The six metallic pillars are identical, with dimensions 0.8 m by 0.8 m (length x width). Both the cargo hold and the factory are metallic structures of large volume. They both form environments that are rich in multipaths. However, more impulsive multipaths are expected within the factory environment since there are usually more metallic

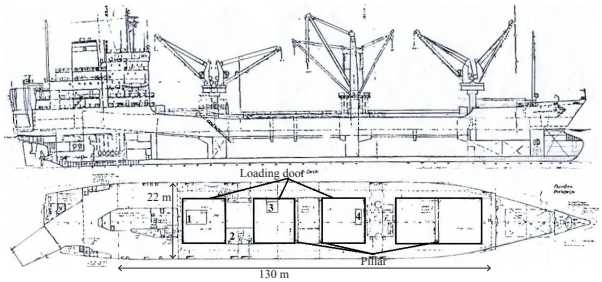

(a)

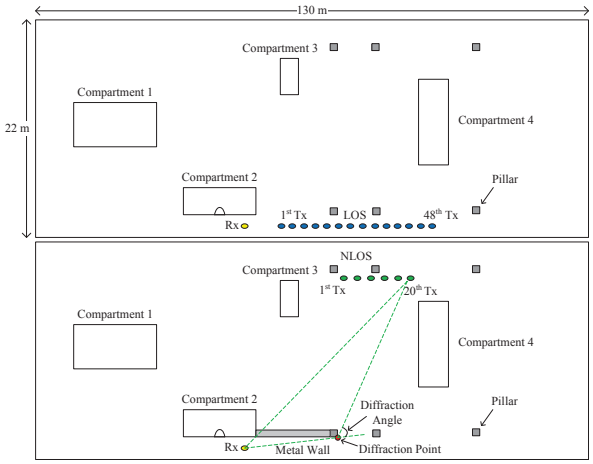

(b)

Fig. 1: (a) Side and top view of the cargo hold. (b) LOS and NLOS measurement setup inside the cargo area.

objects (substructures) such as machineries situated within the factory. The cargo hold is empty during measurement, thus, the metallic walls of the cargo hull acts as an analogous waveguide structure. The channel performance and propagation mode within the two environments are therefore expected to differ. During the measurement campaign, two sets of measurements are conducted within the cargo hold. The first set is the LOS measurement, conducted along one side of the cargo hold. The second set is the NLOS measurement, conducted diagonally across the cargo hold with the LOS path obstructed by a metal wall. Both the LOS and NLOS scenarios are illustrated in Fig. 1(b). The metal wall used in the NLOS measurement is part of the ship's deck that opens downwards into the cargo hold for loading and unloading purposes. The length of this wall is approximately 12.6 m and the width is 1 m.

In a practical sensor network for indoor environment, it has been reported in [16] that the separation between two adjacent sensor nodes (d_{node}) is from 1 to 10 m. Therefore, in the LOS measurement, the transmit antenna is moved away from the receive antenna, with a separation distance from 5.7 to 41.5 m with 48 separation steps along a straight line. This implies that, if a sensor node separation, d_{node}, is assumed to be 5.7 m, then the maximum distance in the LOS setup corresponds to approximately 7 d_{node}. In the NLOS measurement, there is no direct propagation path between the transmitter and receiver due to the presence of the metal wall. For this experimental setup, 20 transmitter to receiver positions are examined. The transmitter is shifted along a straight line as indicated in Fig. 1(b) with increasing distance between the transmitter and the receiver. The distance between the transmitter and the receiver ranges from 21.6 m to 37.9 m. For the same sensor network, the shortest and largest separation for the NLOS setup would correspond to 4 d_{node} and 7 d_{node} respectively. Note that in the LOS experiment, the metal wall is not present.

The measurement system consists of an Agilent VNA and two identical vertically polarized omni-directional discone antennas, AX-71C. The height of the antennas is 2.5 m. For both LOS and NLOS measurements, a step frequency sweep is performed at a centre frequency of 370 MHz. 1601 uniformly distributed frequency steps of continuous waves are transmitted over a bandwidth of 5 MHz. To ensure that the channel is static during a single sweep of the measurement, the minimum sweep time of 111.56 ms is used. With these settings, the minimum resolvable delay is 0.2 μs and the maximum measurable delay is 320.2 μs. For each transmitter to receiver separation, a set of 50 sweeps are taken and logged via a GPIB card onto a laptop. In order to obtain the time domain channel response, the Inverse Fast Fourier Transform (IFFT) of the recorded frequency domain transfer function S21 as shown in (1) and (2) is performed during post processing. The average PDP in the time domain is obtained by taking the average of 50 continuous instantaneous impulse responses. Pre-calibration was performed using the VNA's build-in calibration routine in order to compensate for amplitude and phase distortion. This calibration was done to the point where the cables connect to the antennas. According to [17], if the test environment is rich with scatterers, the physical multipath components will arrive from all possible directions and each resolvable multipath component includes many physical multipath components. The measured channel response will be equivalent to the propagation channel response.

$$S_{21}(\omega) \propto H(\omega) = \frac{Rx(\omega)}{Tx(\omega)} \tag{1}$$

$$h(t) = FT^{-1}[H(\omega)] \tag{2}$$

B. Simulation Setup

The ray-tracing simulator Wireless Insite [18] is used to study and understand the detail channel characteristics of the experimental environment. The 3-D model is simulated through ray-tracing in order to examine the effect of transmission, reflection, and diffraction within the cargo hold. The simulation tool used is based on a hybrid Shooting Bouncing Ray (SBR) algorithm and Geometrical Theory of Diffraction (GTD). The simulation model presented is a simplified model of the actual environment; it is built to be as similar to the actual measurement scenarios as possible. Four compartments and six pillars are modeled within the cargo hold for both the LOS and NLOS scenarios. In the NLOS scenario, there is an additional metal wall modeled within the cargo hold. The models of the cargo hold with its substructures are shown in Fig. 1(b). The material of all the objects is modeled as Perfect Electric Conductor (PEC). The cargo hold, compartments and pillars are modeled as a series of hollow metal boxes while the wall is modeled as a metal plate. Two vertically polarized omni-directional dipoles are used as the transmitting and receiving antennas. In order to maximize the number of output rays, the maximum number of reflections is set to 10, the maximum number of transmissions is set to 6 and the maximum number of diffractions is set to 2. For each simulation, Wireless Insite is able to generate a list of propagation paths (up to 250 rays) and the amplitude associated with each path.

III. Results and Discussion

Fig. 2(a) shows the average PDPs obtained from the shortest and the longest transmitter to receiver distances in both the LOS and the NLOS measurements. For ease of comparison, the arrival times of the first peaks in the PDPs are normalized to 0 μs. From Fig. 2(a), it is found that the difference in power level between the two first peaks in the LOS PDPs is around 10.4 dB. If free space path loss is assumed, the difference in received signal power level should be 17.2 dB. The power difference obtained from the measurement is significantly smaller than that calculated from free space path loss. The main reason for this is the analogous waveguide geometry of the cargo hold. Signals are guided along the cargo hold and reflected by the metallic substructures. These signals arrive within the first peak and sum up constructively resulting in a higher received power as compared to free space path loss. Although it should be noted that, similar to [7], some of the signal arrivals within the first peak are also due to featured niches, columns and edges within the cargo hold.

The guided rays that arrive within the first peak (delay of less than 0.2 μs) are simulated. The visualization of these

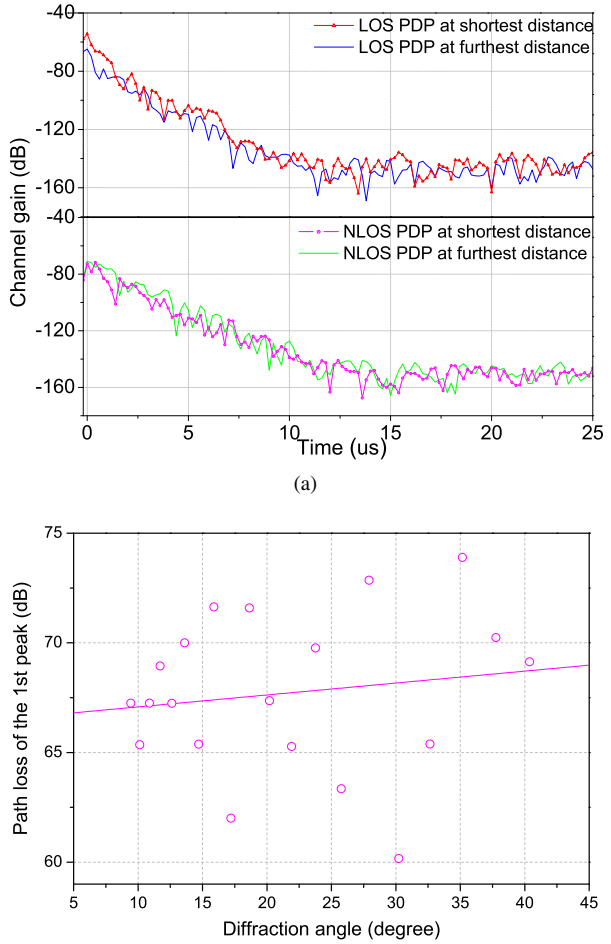

Fig. 2: (a) Power delay profiles from LOS and NLOS measurements. (b) Angular dependency of the shadowing in NLOS measurements.

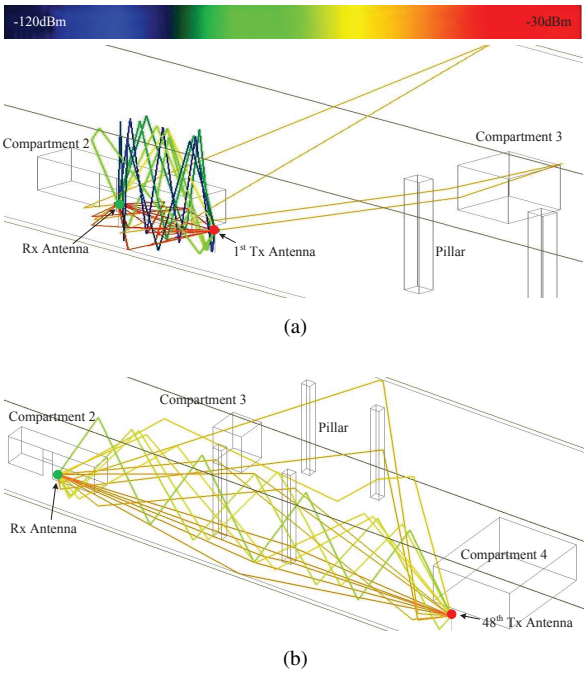

Fig. 3: Visualization for guided signals in the first peak in LOS setup (a) for the shortest distance. (b) for the longest distance.

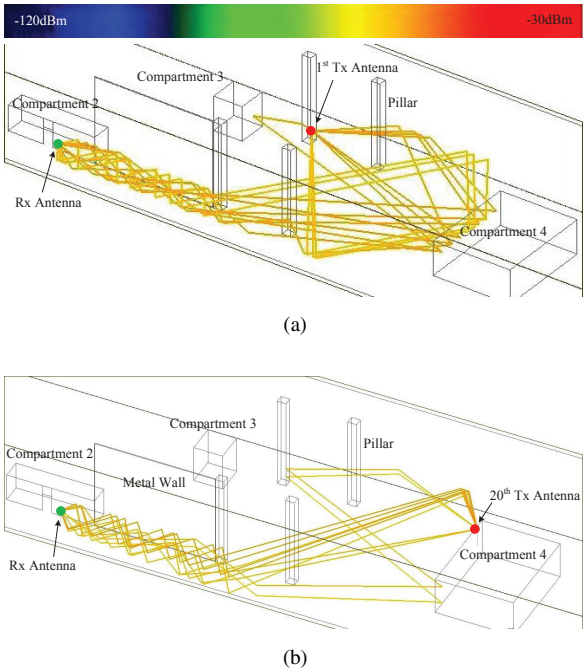

Fig. 4: Visualization for guided signals along the corridor in NLOS setup (a) for the shortest distance. (b) for the longest distance.

rays is provided in Fig. 3. Fig. 3(a) shows all the guided signals arriving within the first peak of the LOS PDP in Fig. 2(a) for the shortest transmitter to receiver distance. Fig. 3(b) shows the guided waves arriving within the first peak of the PDP of LOS measurements shown in Fig. 2(a) for the longest transmitter to receiver distance. It is expected that the number of waves arriving at the receiver within the first peak for the longest distance should be more than that of the shortest distance. However, as observed in Fig. 3, due to the large amount of reflected and diffracted waves, the number of waves arriving at the receiver is similar for both distances.

For PDPs obtained from the NLOS tests shown in Fig. 2(a), it is observed that the signal strength does not drop when the transmitter to receiver distance varies from the shortest (21.6 m) to the longest (38 m). This is due to the shadow regions and the diffraction in the NLOS experimental setup. When the transmitting antenna moves from the first to the twentieth position, although the distance between the transmitter and the receiver is increased, the transmitting antenna is moving out of the shadow region (with a decrease in diffraction angle). Therefore, diffraction loss reduces and a higher channel gain is obtained. The angular dependency of the shadowing effect is shown in Fig. 2(b). The figure shows a plot of the path loss of the first peak versus the diffraction angle. It is observed that the shadowing effect is larger when the diffraction angle is large. The severe shadowing effect due to diffraction is an important propagation mechanism for NLOS propagation. Also observed in this scenario is the analogous waveguide effect due to the presence of the metallic wall. This analogous waveguide effect is clearly observed from the simulation results of the NLOS scenario in Fig. 4. The guiding structure in Fig. 4 is similar to the indoor corridor that has been studied and modelled as a waveguide structure in [19]. Therefore, for the NLOS propagation within the cargo hold,

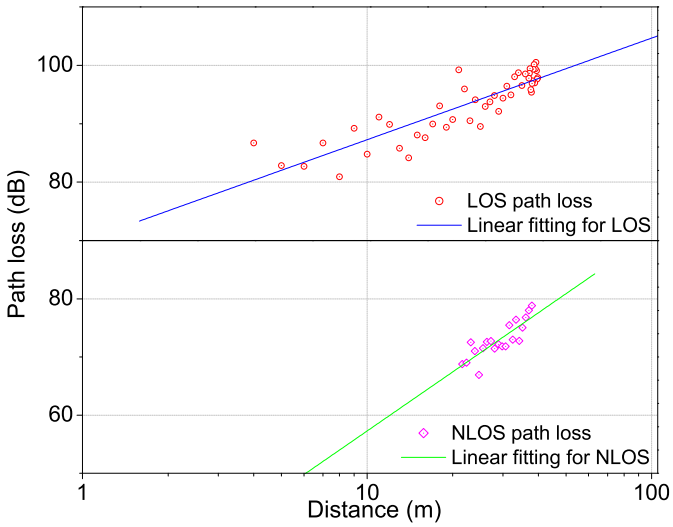

Fig. 5: Propagation loss versus distance and the fitted lines.

the electromagnetic waves are not simply diffracted to the receiver, they are guided along the walls of the cargo hold before being reflected and/or diffracted to the receiver. Due to the small dimension of the analogous waveguide structure, most of these guided signals from the simulations arrive within a short propagation delay of each other. Therefore, these numerous multiple paths that are guided towards the receiver arrive at the receiver with a short time delay and are within the first peak of the PDP in Fig. 2(a).

A. Path Loss for LOS and NLOS Topology

The distance dependent path gain is obtained by taking an average of 50 continuous channel gains. The channel gain is obtained by taking the mean value of the magnitude of 1601 measured complex frequency response points $H(\omega, d)$ over a bandwidth of 5 MHz. The path loss is obtained by adding the antenna gains to the absolute value of the path gain.

$$PL = abs\left(\frac{1}{M \times N}\sum_{j=1}^{N}\sum_{i=1}^{M}|H_{i,j}(\omega)|^2\right) \tag{3}$$

where M is the number of frequency steps in each sweep, and N is the number of continuous sweeps. In this particular experimental setup, $M = 1601$ and $N = 50$. Assuming a classic Log-normal shadowing path loss model, the path loss PL (in dB) at a distance d (in m) can therefore be expressed as:

$$PL(d) = PL(d_0) + 10n\log_{10}\left(\frac{d}{d_0}\right) + X_\sigma \tag{4}$$

where $PL(d_0)$ refers to the path loss in dB at a close range ($d_0 = 1$ m), n is the path loss exponent, and X_σ is a zero-mean Gaussian distributed random variable (in dB) representing shadowing with standard deviation σ (in dB).

$$\text{LOS:} \quad PL = 17 \times \log_{10}(d) + 70 \tag{5a}$$

$$\text{NLOS:} \quad PL = 34 \times \log_{10}(d) + 23 + \text{diffraction loss} \tag{5b}$$

The measured results for the LOS scenario are shown in Fig. 5. A linear fitting with Minimum Mean Squared Error (MMSE) for the path loss is used to fit the measured data. This linear fitting model is given in (5a) where the path loss exponent is found to be 1.7 and the standard deviation (σ) of shadowing is found to be 2.6 dB. The path loss exponent of 1.7 verifies that the cargo hold environment is heavily cluttered. The highly reflective and diffractive nature of the structures of the cargo hold makes it a multipath rich environment. Therefore, a path loss exponent of less than 2 for free space path loss is obtained. In [7], the dual-slope path loss model was used to model the path loss along the cabins' corridor. The path loss in the near region of up to the break point distance of 70 m was found to be less than 2, whereas the path loss in the far region, beyond the break point distance was found to be less than 0.5. This was reported to be due to the guiding effect of the corridor. For this cargo hold, due to the large dimension of the structure, the break point distance is 597 m. Therefore, all measurements are carried out in the near region, before the break point distance. Thus the obtained path loss exponent is 1.7. Similar results were reported in [10]–[12], where path loss exponents of less than 2 were obtained from LOS measurements inside different factory halls at different frequencies due to the cluttered nature of the environment. The small standard deviation (σ) of shadowing (2.6 dB) indicates that shadowing does not play an important role in the LOS propagation within the cargo hold environment. As reported in [11], severe shadowing ($\sigma > 10$ dB) occurs when the receiver is situated a few meters behind a metal obstacle that is much taller than the receiving antenna.

As shown in Section III-A, diffraction by the edge of the metal wall is the primary propagation mode for NLOS propagation in this particular setup. As the position of the transmitting antenna varies, the diffraction loss varies accordingly. To compensate for this diffraction loss, the knife-edge diffraction model is used to calculate the diffraction loss. This loss is then subtracted from the measured path loss values. The obtained path loss for the NLOS scenario together with its linear fitting with MMSE is then plotted in Fig. 5. The linear fit for the NLOS scenario is given in (5b), where the "diffraction loss" is calculated based on knife edge diffraction. The path loss exponent for the NLOS scenario is 3.4 and the standard deviation (σ) of shadowing is 1.7 dB. This path loss exponent of larger than 2 is expected and indicates that the environment is complex and cluttered. In [10], the path loss exponent for lightly cluttered NLOS links is found to range from 2.2 to 3.2, and the path loss exponent for heavily cluttered NLOS links is found to range from 3.7 to 4.5. In [11], the path loss exponent for obstructed links with light clutter and heavy clutter derived from measurement data in five different factories are 2.4 and 2.8 respectively. The path loss exponent of 3.4 obtained here is similar to those of a heavily cluttered environment reported in the literature.

The path loss exponent derived in this section can be used in the design of a sensor network. The maximum distance between sensor nodes and the number of links can be derived. The existing sensor networks using ZigBee technology has a maximum data rate of 250 kbps when operating at 2.4 GHz using OQPSK modulation [20]. Assume that each sensor node transmits a power of 1mW (0 dBm) at the maximum data rate in this design; the thermal noise can be estimated using KTB.

TABLE I: Number of Multirate Components

Threshold	10 dB	13 dB	15 dB	20 dB
LOS	17.3	15.5	15.0	13.4
NLOS	19.7	18.1	17.3	15.8

If a 10 dB SNR, a 10 dB fading margin, and a 5.7 m sensor node spacing is assumed, then, for the LOS scenario within the cargo hold, the maximum achievable distance calculated from (5a) is 85 m, with an estimated adjacent sensor node connections of 15 links. For the NLOS scenario, taking into consideration a maximum knife-edge diffraction loss of 27.7 dB; the maximum achievable distance calculated from (5b) is 34 m; with an estimated adjacent sensor node connections of 6 links.

B. Small-scale Multipath Effect for LOS and NLOS

In the previous two sections, it has been shown that besides the direct path in the LOS topology and diffraction in the NLOS topology, the bulk of the received power is a summation of numerous multipath components resulting from multiple reflections by the metallic cargo hold and its substructures. In this section, small-scale channel characteristics for both LOS and NLOS scenarios are presented and compared. In part 1, the number of multipath components is examined.

1) Number of Multipath Components: Table I lists the mean number of multipath components obtained from 48 LOS measurement locations and 20 NLOS measurement locations for four different threshold levels. The four threshold levels are 10 dB, 13 dB, 15 dB and 20 dB above the noise floor. The minimum threshold used is 10 dB above the noise floor (10 dB SNR). This is because the standard deviation of the noise floor is about 6 dB for both sets of measurements. From Table I, it can be seen that the number of multipath components decreases gradually as the threshold increases from 10 dB SNR to 20 dB SNR for both the LOS and NLOS results. This is mainly due to the diffusive nature of the multipath components.

The difference in the mean number of multipath components between the LOS scenario and the NLOS scenario is insignificant. This is because most of the multipath components are due to waves reflected and guided by the cargo hold and its substructures, which are common to both LOS and NLOS scenarios. Therefore, it can be deduced that the number of multipath components is probably independent of line-of-sight availability.

The following analysis is done based on a threshold of 10 dB SNR since it captures the most amount of channel information. The number of multipath components, Num, is fitted using a linear relationship with the transmitter to receiver separation, d (in m). Therefore, two linear models (6a) and (6b) are obtained for the LOS and the NLOS scenarios, respectively. From the small slopes with absolute value of less than 0.05, in (6a) and (6b), it can be concluded that the number of multipath components is almost independent of the transmitter to receiver separation, d for both LOS and NLOS scenarios. This is not surprising, since it was reported in [21] that the statistics of the measured number of multipath components is comparable in LOS and NLOS topographies for a spacious, open plan industrial area. The cargo hold environment is similar to the environment reported in [21]. The average number of multipath components is also found to be similar to those obtained in [21]. In order to study the behavior of these multipath components, the rate of decay of these multipath components will be modelled.

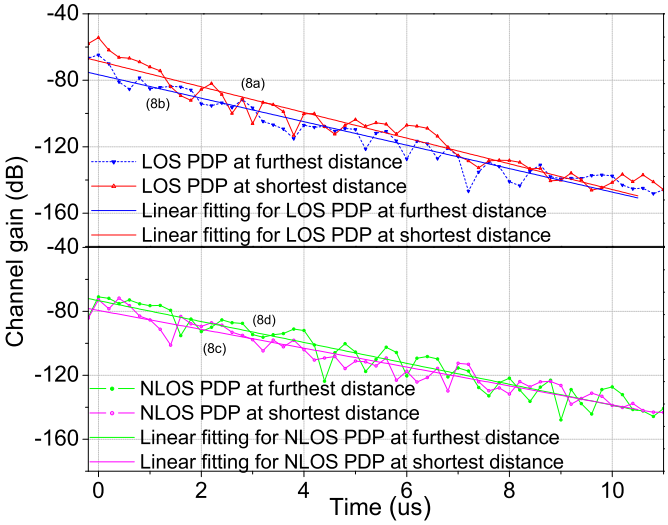

Fig. 6: Average PDPs and associated linear fittings for LOS and NLOS scenarios

$$\text{LOS}: \quad Num = 0.013d + 17 \tag{6a}$$

$$\text{NLOS}: \quad Num = -0.037d + 21 \tag{6b}$$

2) Multipath Strength vs. Delay: PDPs are commonly modeled using the exponential function [22]–[25]. For example, in [22], the shape of the average PDPs obtained from LOS channels in a passengers' cabin of an aircraft is modeled using a simple exponential decay function (7), where γ is the exponential decay constant, a_k and τ_k are defined as the amplitude and the arrival time of the k^{th} arrival signal respectively. The random significant impulses within the first 30 ns in the PDPs were reported to be due to specular reflection from the cabin bulkhead or deck.

$$E\{|a_k|^2\} \propto \exp\left(\frac{-\tau_k}{\gamma}\right) \tag{7}$$

Besides using the exponential function, in [26], the PDP for propagation along a street at 2.6 GHz was also calculated based on the waveguide theory. In [27], the structure of the PDP matches the empirical power law model (power is linearly proportionate to $10\log_{10}(t)$, where t is the arrival time of signals). In this paper, a linear relationship is proposed to model the structure of the average PDPs obtained in an analogous waveguide environment. The linear model with MMSE is used to fit the average PDPs given in Fig. 2(a). It is shown in Fig. 6 that the proposed linear model can describe the trend of the PDPs well. The corresponding linear fits for the shortest and the furthest distance in LOS and NLOS scenarios are provided in (8a) to (8d) where P represents the average channel gain in dB and t represents the time delay in μs. The slope of the linear models for the average PDPs from the shortest distance and the furthest distance in LOS scenarios

are -7.7 dB/μs and -7.1 dB/μs respectively; while those in NLOS scenarios are -5.9 dB/μs and -6.5 dB/μs respectively. It is found that the slope is higher when the first arrival signals have higher amplitudes, i.e. at the shortest distance in the LOS scenario, since the reflected signals with long delays are of similar amplitudes in all scenarios. Although the difference in slope is not significant, the slopes from LOS scenarios are higher since the amplitude of the first arrival signals are generally higher for LOS scenarios than NLOS scenarios. The guiding effect/multiple reflection from the cargo hold and its substructures is a significant propagation mode and is common to both the LOS and the NLOS measurement scenarios.

$$\text{LOS with } D_{min}: \quad P = -7.7t - 68 \tag{8a}$$
$$\text{LOS with } D_{max}: \quad P = -7.1t - 77 \tag{8b}$$
$$\text{NLOS with } D_{min}: \quad P = -5.9t - 79 \tag{8c}$$
$$\text{NLOS with } D_{max}: \quad P = -6.5t - 73 \tag{8d}$$

In such cluttered environment, the linear model is capable of describing the structure of the average PDPs. In order to further examine the validity of this statement, the linear fitting is applied to the average PDPs obtained from passengers' cabin in [22]. Similar to the cargo hold, this passengers' cabin is also a waveguide like structure that is cluttered with seats and baggage compartments. In the passengers' cabin, signals also arrived at the receiver through multiple reflections via the corridor and the walls of the cabin. The cabin in [22] and the cargo hold structure in this paper are both analogous waveguide structures with highly reflective substructures. Therefore, the proposed linear model should also be able to fit the PDPs obtained from the passengers' cabin. The average PDPs obtained from propagation inside the passengers' cabin presented in [22] is shown in Fig. 7. A linear fitting is used to fit the average PDPs for 3 different scenarios within the passengers' cabin. As shown in Fig. 7, the linear model is sufficient to describe the structure of the PDPs, since the multipath signals resulting from multiple reflections within the passengers' cabin are mainly diffusive. This verifies that the linear model is suitable for the modeling of multipath components in a confined cluttered environment with reflective materials.

3) RMS Delay Spread: The RMS delay spread takes into consideration both the amplitude and time delay of the multipath components from average PDPs. It is defined as the square root of the second central moment of the average PDP. The calculated RMS delay spread values for a threshold level of 10 dB above noise floor (10 dB SNR) are plotted against the distance between the transmitter and the receiver in Fig. 8. For the LOS measurements, the delay spread increases as distance increases. This is because although there is minimum increase in the number of multipath components with an increase in distance, the signal strength of the multipath components decreases with an increase in distance. After a distance of about 38 m, the delay spread tapers off, since the signal strength of the multipath components also tapers off and becomes a constant. However, because of the random appearance of multipath components at large distances, the delay spread appears random. For NLOS measurements, the delay spread does not follow any obvious trend with the increase in distance. By

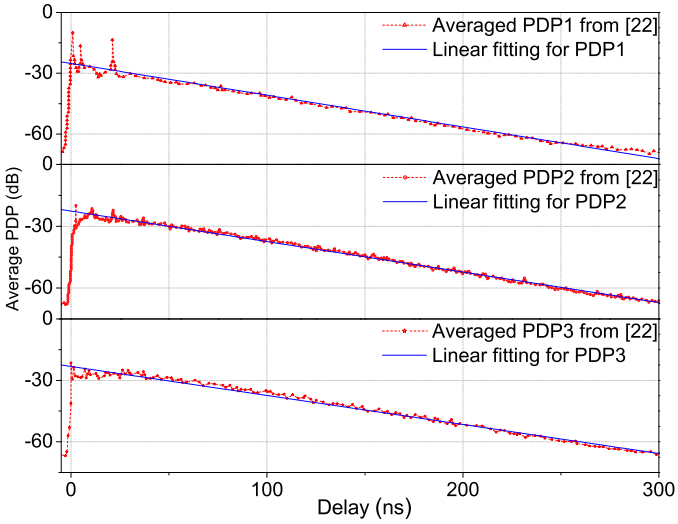

Fig. 7: Extracted average PDPs and associated linear fittings from when receiving antenna is mounted at row 19 on headrest (PDP1), on the outboard armrest (PDP2) and on the footrest (PDP3) in Boeing 737 from [22].

comparing the delay spread obtained from LOS and NLOS measurements in Fig. 8, it can be seen that the delay spread is generally higher for the NLOS scenarios. This is because multipath signals strengths are relatively high compared to the obstructed line of sight signal strength (first arrival signal) in the NLOS scenario. The difference in the number of multipath components and their corresponding signal strengths for both scenarios is shown in the measurement PDP results in Fig. 2(a).

The average RMS delay spread value is 374 ns for the 48 LOS links and 602 ns for the 20 NLOS links. In [12], the RMS delay spread value obtained from the five factories with sizes ranging from 21k m^2 to 150k m^2, is between 30 ns to 300 ns. The size of the cargo hold is 3k m^2, which is significantly smaller than those reported in [12]. However, the distance between the transmitter and the receiver in the measurements is comparable. The larger delay spread obtained from the cargo hold is due to the rich multipath environment as a result of the metallic box-like structure. By taking the coherence bandwidth as the bandwidth over which the frequency correlation function is above 0.5, the maximum usable data rates (assuming BPSK) for LOS and NLOS channels are found to be 0.53 and 0.33 Mbps respectively. Therefore, the maximum usable symbol rate for channels inside the cargo hold of the merchant ship is 330 kbps if no equalizer is used. The achieved data rate is enough for voice and data communication; i.e., voice encoded with GSM 6.10 codec (15 kbps) and moderate frame-rate, low resolution color video (256 kbps) [24]. For existing wireless sensor networks based on ZigBee technology, the maximum data rate is 250 kbps (OQPSK), 20 kbps (BPSK) and 40 kbps (BPSK) at 2.4 GHz, 868 MHz and 915 MHz respectively. Besides these three bands, the IEEE802.15.4C study group is now considering the use of another three newly opened bands in China, 314-316 MHz, 430-434 MHz, and 779-787 MHz [28]. Since the multipath components within the cargo hold is mainly due to the guiding effect of its analogous waveguide structure, the delay spread is expected

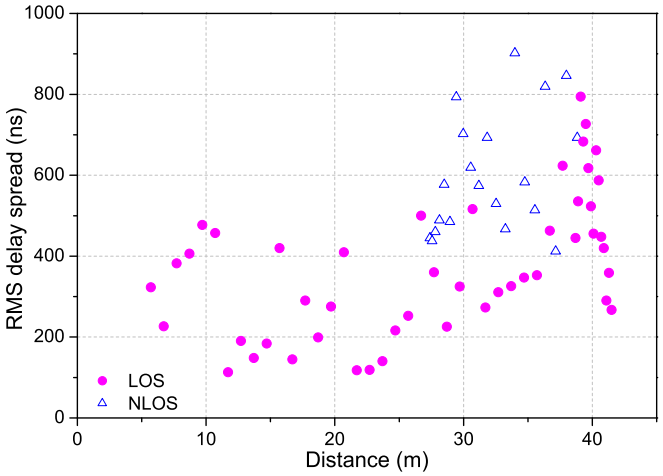

Fig. 8: RMS delay spread versus distance.

to be similar regardless of frequency. The minimum data rate found for the cargo hold environment is 330 kbps, therefore, it is possible to deploy a wireless sensor network in the cargo hold environment.

IV. Conclusion

In this paper, the propagation mechanisms inside a cargo hold of a merchant ship are studied for both LOS and NLOS topologies. 3-D ray-tracing simulations are used to examine the propagation modes obtained from the measurement results. It is found that the guiding effect and the multiple reflections via the cargo hold and its substructures is an important propagation mechanism for both LOS and NLOS communication within the cargo hold. Path loss models using linear regression have been derived for the cargo hold environment. Path loss exponents of 1.7 for LOS topology and 3.4 for NLOS topology are recommended. The shadowing effect is found to be insignificant in this metallic environment since the height of the antenna (2.5 m) is comparable to the height of the obstacle (5 m) as explained in [11]. Based on the fitted path loss model, the number of links that can be established between adjacent nodes are estimated and it was concluded that wireless sensor network can be implemented in the cargo hold.

Small-scale channel characteristics analysis and comparison for the LOS and the NLOS scenarios are presented. It can be concluded that, although the first signal arrival has higher received power for LOS propagation, both LOS and NLOS propagation paths experience similar multipath fading. This is verified through the examination of the number of multipath components and the linear decay trend of the multipath signals' strength with respect to the arrival times. It is found that the number of multipath components is independent of distance for both LOS and NLOS scenarios. Furthermore, the decay trends of the multipath components for both LOS and NLOS can be described using a linear function. The linear model is also used to fit the results from a similar confined waveguide structure-like cluttered environment of a passengers' cabin from the literature. For highly reflective enclosed environment such as cargo holds, passenger cabins or industrial halls, the linear model provides a good representation of the power decay of multipath components due to the linearly decaying reflection loss of the multipath components. Finally, another important small-scale fading parameter, the RMS delay spread is presented. Due to the highly reflective and cluttered environment, the delay spread values obtained in the cargo hold are larger than those reported in literature. Average RMS delay spread values of 374 ns and 602 ns are obtained for LOS and NLOS topologies, respectively. With a correlation coefficient of 0.5, the maximum usable data rate is approximately 330 kbps if no equalization is used. This is sufficient for real time voice or low resolution video communication for wireless sensor monitoring systems. The proposed models are useful for the design of wireless sensor networks within the cargo hold for tracking and monitoring applications. These models can also be used for the simulation of a realistic metallic, cluttered, and enclosed environment. However, since the presented results are for an empty cargo hold, further research needs to be performed for a partially loaded or completely loaded cargo hold.

References

[1] Y. Zhang, S. Xing, P. Xu, and X. Wang, "Shipping containers of dangerous goods condition monitoring system based on wireless sensor network," in *Proc. 2010 International Conf. on Networked Computing*, pp. 1–3.

[2] D. R. J. Estes, T. B. Welch, A. A. Sarkady, and H. Whitesel, "Shipboard radio frequency propagation measurements for wireless networks," in *Proc. 2001 Military Communication Conf.*, pp. 247–251.

[3] E. L. Mokole, M. Parent, T. T. Street, and E. Tomas, "RF propagation on EX-USS Shadwell," in *Proc. 2000 IEEE-APS Conf. on Antennas and Propagation for Wireless Communications*, pp. 153–156.

[4] P. Nobles and L. R. Scott, "Wideband propagation measurements onboard HMS Bristol," in *Proc. 2003 Military Communication Conf.*, pp. 1412–1415.

[5] E. Balboni, J. Ford, R. Tingley, K. Toomey, and J. Vytal, "An empirical study of radio propagation aboard naval vessels," in *Proc. 200 IEEE-APS Conf. on Antennas and Propagation for Wireless Communications*, pp. 157–160.

[6] A. Mariscotti, M. Sassi, A. Qualizza, and M. Lenardon, "On the propagation of wireless signals on board ships," in *Proc. 2010 IEEE Instrumentation and Measurement Technology Conf.*, pp. 1418–1423.

[7] A. Mariscotti, "Experimental determination of the propagation of wireless signals on board a cruise ship," *Measurement*, vol. 44, pp. 743–749, May 2011.

[8] X. H. Mao, Y. H. Lee, and B. C. Ng, "Wideband channel characterization along lift shaft onboard a ship," in *Proc. 2010 IEEE Antennas and Propagation Society International Symposium*, pp. 1–4.

[9] X. H. Mao, Y. H. Lee, and B. C. Ng, "Wideband channel characterization along lift shaft onboard a ship," in *Proc. 2009 IEEE Antennas and Propagation Society International Symposium*, pp. 1–4.

[10] E. Tanghe, W. Joseph, L. Verloock, L. Martens, H. Capoen, K. Van Herwegen, and W. Vantomme, "The industrial indoor channel: large-scale and temporal fading at 900, 2400, and 5200 mhz," *IEEE Trans. Wireless Commun.*, vol. 7, pp. 2740–2750, July 2008.

[11] T. S. Rappaport and C. D. McGillem, "UHF fading in factories," *IEEE Trans. Sel. Areas Commun.*, vol. 7, pp. 40–48, Jan. 1989.

[12] T. S. Rappaport, "Characterization of UHF multipath radio channels in factory buildings," *IEEE Trans. Antennas Propagat.*, vol. 37, pp. 1058–1069, Aug. 1989.

[13] S. Kjesbu and T. Brunsvik, "Radiowave propagation in industrial environments," in *Proc. 2000 Conf. of the IEEE Industrial Electronics Society*, pp. 2425–2430.

[14] A. Miaoudakis, A. Lekkas, G. Kalivas, and S. Koubias, "Radio channel characterization in industrial environments and spread spectrum modem performance," in *Proc. 2005 IEEE Conf. on Emerging Technologies and Factory Automation*, pp. 19–25.

[15] D. Hampicke, A. Richter, A. Schneider, G. Sommerkorn, R. S. Thoma, and U. Trautwein, "Characterization of the directional mobile radio channel in industrial scenarios, based on wide-band propagation measurements," in *Proc. 1999 IEEE Vehicular Technology Conf.*, pp. 2258–2262.

[16] Avalilable: http://www.automatedbuildings.com/news/dec04/articles/kele/zebrick.htm.
[17] S. Chiu and D. G. Michelson, "Effect of human presence on UWB radiowave propagation within the passenger cabin of a midsize airliner," *IEEE Trans. Antennas Propagat.*, vol. 58, pp. 917–926, Aug. 2010.
[18] Available: http://www.remcom.com/wirelessinsite.
[19] D. Porrat and D. C. Cox, "UHF propagation in indoor hallways," *IEEE Trans. Wireless Commun.*, vol. 3, pp. 1188–1198, July 2004.
[20] Available: http://en.wikipedia.org/wiki/ZigBee.
[21] T. S. Rappaport, S. Y. Seidel, and K. Takamizawa, "Statistical channel impulse response models for factory and open plan building radio communication system design," *IEEE Trans. Commun.*, vol. 39, pp. 794–807, May 1991.
[22] S. Chiu, J. Chuang, and D. G. Michelson, "Characterization of UWB channel impulse responses within the passenger cabin of a boeing 737-200 aircraft," *IEEE Trans. Antennas Propagat.*, vol. 58, pp. 935–945, Mar. 2010.
[23] H. Hashemi, "The indoor radio propagation channel," *Proc. IEEE*, vol. 81, pp. 943–968, July 1993.
[24] T. Bronez and J. Marshall, "Shipboard experiments for a multihop 802.11 communications system—RF channel characterization and MAC performance measurement," in *Proc. 2005 Military Communications Conf.*, pp. 557–563.
[25] A. F. Molisch, D. Cassioli, C. C. Chong, S. Emami, A. Fort, B. Kannan, J. Karedal, J. Kunisch, H. G. Schantz, K. Siwiak, and M. Z. Win, "A comprehensive standardized model for ultrawideband propagation channels," *IEEE Trans Antennas Propagat.*, vol. 54, pp. 3151–3166, Nov. 2006.
[26] D. Porrat and D. C. Cox, "Delay spread in microcells analysed with waveguide theory," in *Proc. 2002 IEEE Vehicular Technology Conf.*, pp. 512–516.
[27] S. Ichitsubo, T. Furuno, and R. Kawasaki, "A statistical model for microcellular multipath propagation environment," in *Proc. 1997 IEEE Vehicular Technology Conf.*, pp. 61–66.
[28] A. Sikona, "The ZigBee architecture—an introduction," in *Proc. 2010 European ZigBee Developers' Conf.*, pp. 1–40.

Xiao Hong Mao received the B. Eng. (Hons) in Electrical and Electronics Engineering from the Nanyang Technological University, Singapore, in 2007, where she is working towards the Ph.D. degree. She has been a Research Engineer in the School of Electrical and Electronic Engineering, Nanyang Technological University since September 2009. Her research interest is in channel modeling and characterization in complex environments.

Yee Hui Lee received the B. Eng. (Hons) and M. Eng. degrees in Electrical and Electronics Engineering from the Nanyang Technological University, Singapore, in 1996 and 1998, respectively. She received her Ph.D. degree from the University of York, York, U.K., in 2002. Since July 2002, she has been an Associate Professor at the School of Electrical and Electronic Engineering, Nanyang Technological University. Her interest is in channel characterization, rain propagation, antenna design, electromagnetic band gap structures, and evolutionary techniques.